Published for SISSA by Springer

Received: *March 19, 2017*
Revised: *May 24, 2017*
Accepted: *June 5, 2017*
Published: *June 13, 2017*

A new formulation of Lee-Wick quantum field theory

Damiano Anselmi and Marco Piva

Dipartimento di Fisica "Enrico Fermi", Università di Pisa,
Largo B. Pontecorvo 3, 56127 Pisa, Italy
INFN, Sezione di Pisa,
Largo B. Pontecorvo 3, 56127 Pisa, Italy

E-mail: damiano.anselmi@unipi.it, marco.piva@df.unipi.it

Abstract: The Lee-Wick models are higher-derivative theories that are claimed to be unitary thanks to a peculiar cancelation mechanism. In this paper, we provide a new formulation of the models, to clarify several aspects that have remained quite mysterious, so far. Specifically, we define them as nonanalytically Wick rotated Euclidean theories. The complex energy plane is divided into disconnected regions, which can be related to one another by a well-defined, albeit nonanalytic procedure. Working in a generic Lorentz frame, the models are intrinsically equipped with the right recipe to treat the pinchings of the Lee-Wick poles, with no need of external ad hoc prescriptions. We describe these features in detail by calculating the one-loop bubble diagram and explaining how the key properties generalize to more complicated diagrams. The physical results of our formulation are different from those of the previous ones. The unusual behaviors of the physical amplitudes lead to interesting phenomenological predictions.

Keywords: Beyond Standard Model, Models of Quantum Gravity

ArXiv ePrint: 1703.04584

doi:10.1007/JHEP06(2017)066

JHEP06(2017)066

Contents

JHEP06(2017)066

1 Introduction

The Lee-Wick (LW) models are special higher-derivative theories, defined in a peculiar way, which are claimed to lead to a perturbatively unitary S matrix [1–3]. Precisely, the claim is that they are equipped with well defined cutting equations [4–7], such that if we project the initial and final states onto the subspace V of physical degrees of freedom, only states belonging to the same space V propagate through the cuts. Several properties of the models and aspects of their formulation have not been clarified exhaustively, so far. In this paper we plan to overcome those problems by reformulating the theories completely.

It is well known that higher-derivative kinetic Lagrangian terms may improve the ultraviolet behaviors of the Feynman diagrams and may turn nonrenormalizable theories into renormalizable ones, as in the case of higher-derivative gravity [8, 9]. However, the higher-derivative corrections, if not treated properly, lead to violations of unitarity or even mathematical inconsistencies [10]. The Lee-Wick idea is promising, because it claims to reconcile renormalizability and unitarity.

The propagators of the LW models contain extra poles, which we call *LW poles*, in addition to the poles corresponding to the physical degrees of freedom and the poles corresponding to the gauge degrees of freedom (such as the longitudinal and temporal components of the gauge fields and the poles of the Faddeev-Popov ghosts). The LW poles come in complex conjugate pairs, which we call *LW pairs*. Cutkosky et al. (CLOP) showed in ref. [3] that the S matrix is not analytic when pairs of LW poles pinch the integration

path on the energy. Analyticity is a property we are accustomed to, but not a fundamental physical requirement. Nakanishi [11] showed that, if defined in a certain way, the models violate Lorentz invariance. This problem is more serious, but it can be avoided by defining the theories in a different way. In ref. [3] it was proposed to treat the pinching of the LW poles by means of a procedure of limit, which is known as *CLOP prescription*. In simple situations, the CLOP prescription gives an unambiguous, Lorentz invariant and unitary result, as confirmed by the calculations of Grinstein et al. [12] in the case of the bubble diagram. However, it is not clear how to incorporate the CLOP prescription into a Lagrangian and ambiguities are expected in high-order diagrams [3]. Thus, some key issues concerning the formulation of the LW models have remained open and are awaiting to be clarified.

It is more convenient to change approach and define the LW models as nonanalytically Wick rotated Euclidean higher-derivative theories. First, we know from ref. [10] that a Minkowski formulation of such types of higher-derivative theories is not viable, since in general it generates nonlocal, non-Hermitian divergences that cannot be removed by any standard approach. The Wick rotation from the Euclidean framework is thus expected to play a crucial role, because it is the only viable path.

However, the Wick rotation of the higher-derivative theories we are considering turns out to be nonanalytic, because of the LW pinching, to the extent that the complex energy plane is divided into disjoint regions of analyticity. The Lorentz violation is avoided by working in a generic Lorentz frame, with generic external momenta, deforming the integration domain on the loop space momenta in a suitable way and then analytically continuing in each region separately. We show that, if we do so, the models are intrinsically equipped with all that is necessary to define them properly. In particular, there is no need of the CLOP prescription, or any other prescription to handle the pinching of the LW poles. Actually, the CLOP prescription should be dropped, because it leads to ambiguities, even in a simple case such as the bubble diagram with different physical masses.

The behaviors of the amplitudes show some unexpected features, which lead to interesting phenomenological predictions. In particular, the violation of analyticity is quite apparent, when the amplitude is plotted. If ever observed, this behavior could be the quickest way to determine the experimental value of the energy scale M associated with the higher-derivative terms, which is the key physical constant of the LW models.

Indeed, the Lee-Wick models have been also studied for their possible physical applications, which include QED [2], the standard model [13–16], grand unified theories [17, 18] and quantum gravity [19–22].

The paper is organized as follows. In section 2, we outline the formulation of the LW models as nonanalytically Wick rotated Euclidean theories. In section 3 we study the LW pinching in detail, in the case of the bubble diagram. In particular, we show how Lorentz invariance is recovered in each region of the complex energy plane. In section 4, we describe the calculations of the physical amplitudes in a neighborhood of the LW pinching and show that the CLOP and similar prescriptions are ambiguous and not consistent with our approach. In section 5 we evaluate the bubble diagram in the new formulation and show that the physical results are in general different from those that follow from the CLOP and other prescriptions. We also comment on the phenomenological relevance of

JHEP06(2017)066

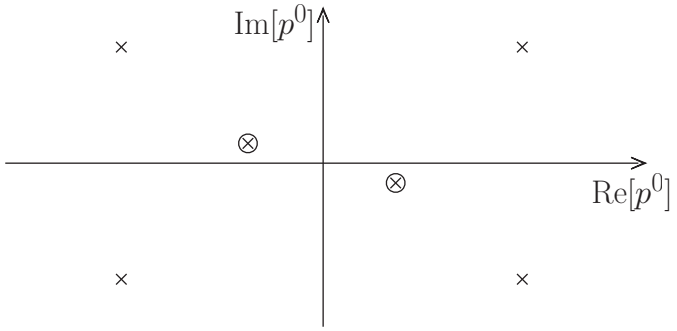

Figure 1. Poles of the propagator.

the results. In section 6 we explain why the basic properties of our formulation generalize to more complicated diagrams.

2 Lee-Wick models as Wick rotated Euclidean theories

In this section we outline the new formulation of the LW models. We begin by describing the class of higher-derivative theories that we are considering. The higher-derivative Lagrangian terms are multiplied by inverse powers of certain mass scales, which we call *LW scales*. For simplicity, we can assume that there is just one LW scale, which we denote by M, since the generalization to many LW scales is straightforward.

When M tends to infinity, the propagators must tend to the ones of ordinary unitary theories. Moreover, the extra poles that are present when $M < \infty$ must come in complex conjugate pairs and satisfy $\mathrm{Re}[p^2] \geqslant 0$, $\mathrm{Im}[p^2] \neq 0$.

A typical propagator of momentum p is equal to the standard propagator times a real function of p^2 that has no poles on the real axis. For concreteness, we take

$$iD(p^2, m^2, \epsilon) = \frac{iM^4}{(p^2 - m^2 + i\epsilon)((p^2)^2 + M^4)}. \tag{2.1}$$

More general propagators can be considered. In particular renormalization may lead to structures such as

$$\frac{iM^4}{(p^2 - m^2 + i\epsilon)((p^2 - \mu^2)^2 + M^4)}.$$

However, the key features are already encoded in (2.1) and the extension does not change the sense of our investigation.

The poles of (2.1) are

$$p^0 = \pm\omega_m(\mathbf{p}) \mp i\epsilon, \qquad p^0 = \pm\Omega_M(\mathbf{p}), \qquad p^0 = \pm\Omega_M^*(\mathbf{p}), \tag{2.2}$$

where $\omega_m(\mathbf{p}) = \sqrt{\mathbf{p}^2 + m^2}$ and $\Omega_M(\mathbf{p}) = \sqrt{\mathbf{p}^2 + iM^2}$. Their locations are shown in figure 1, where the LW poles are denoted by means of an $\times$, while the standard poles are denoted by a circled $\times$.

We can integrate p^0 along the real axis or along the imaginary axis. The first choice defines the Minkowski theory, the second choice defines the Euclidean theory. The two give

JHEP06(2017)066

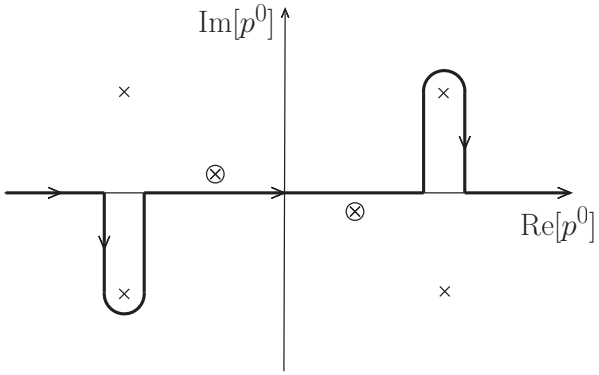

Figure 2. The Lee-Wick integration path.

different results, because, even if the integration path at infinity does not contribute, some poles are located in the first and third quadrants of the complex plane. In ref. [10] it was shown that in general the Minkowski theories of this type are inconsistent, because they are plagued with nonlocal, non-Hermitian divergences that cannot be subtracted away without destroying the basic properties of the theory. The bubble diagram in four dimensions is one of the few convergent exceptions, but it becomes nonlocally divergent as soon as nontrivial numerators are carried by the vertices, which happens for example in higher-derivative gravity. This fact forces us to proceed with the Euclidean theory.

Usually, the Wick rotation is an analytic operation everywhere, but in the Lee-Wick models it is analytic only in a region of the complex energy plane, the one that contains the imaginary axis. We call it *main region* and denote it by $\mathcal{A}_0$. The complex plane turns out to be divided into several disconnected regions $\mathcal{A}_i$, which can be reached from the main region in a nonanalytic way. The regions $\mathcal{A}_i$ are called *analytic regions*.

In the light of this fact, the calculation of the correlation functions proceeds as follows. The loop integrals are evaluated at generic (possibly complex) external momenta, in each analytic region $\mathcal{A}_i$ of the complex plane. For a reason that we will explain, we anticipate that it is also necessary to work in a sufficiently generic Lorentz frame, because special Lorentz frames may squeeze entire regions to lines and make the calculation ill defined. The $\mathcal{A}_i$ subdomain where the calculation is done is denoted by $\mathcal{O}_i$ and has to satisfy suitable properties. For example, it must contain an accumulation point.

In general, Lorentz invariance and analyticity are lost in the intermediate steps, in all the regions $\mathcal{A}_i$ apart from the main one. They are recovered by deforming the integration domain on the loop space momenta in a nontrivial way. After the evaluation, the amplitude is analytically continued from $\mathcal{O}_i$ to the rest of the region $\mathcal{A}_i$. This procedure gives the amplitude of the LW model, region by region. Since it is not possible to relate the regions analytically, the Wick rotation is nonanalytic. Yet, the regions are related by a well-defined nonanalytic procedure, which we describe in the next sections.

We may condense their articulated definition by saying that *the LW models are non-analytically Wick rotated Euclidean higher-derivative theories of a special class.*

JHEP06(2017)066

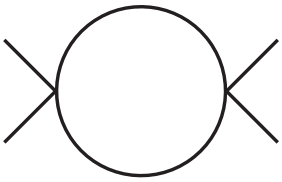

Figure 3. Bubble diagram.

Consider the propagator (2.1) and its poles (2.2). When the imaginary axis is rotated to the real one, we get the integration path shown in figure 2. The Wick rotation is less trivial when performed in Feynman diagrams. To be explicit, consider the bubble diagram (figure 3). It has two propagators, so the number of poles doubles. If one propagator has momentum k and the other propagator has momentum $k-p$, in D spacetime dimensions we have a loop integral proportional to

$$\mathcal{J}(p) = \int \frac{\mathrm{d}^D k}{(2\pi)^D} D(k^2, m_1^2, \epsilon_1) D((k-p)^2, m_2^2, \epsilon_2), \tag{2.3}$$

the associated amplitude being $\mathcal{M}(p) = -i\lambda^2 \mathcal{J}(p)/2$, where λ is the coupling and $1/2$ is the combinatorial factor. When we vary the external momentum p, the poles of the first propagator are fixed [given by formula (2.2) with $p \to k$, $m \to m_1$], while those of the second propagator, which are

$$k^0 = p^0 \pm \omega_{m_2}(\mathbf{k}-\mathbf{p}) \mp i\epsilon, \qquad k^0 = p^0 \pm \Omega_M(\mathbf{k}-\mathbf{p}), \qquad k^0 = p^0 \pm \Omega_M^*(\mathbf{k}-\mathbf{p}), \tag{2.4}$$

move on the complex k^0 plane. With respect to the fixed poles, this sextet of poles is translated by p^0 and deformed by $\mathbf{p}$. At some point, the translation makes some poles cross the imaginary axis, which is the integration path. To preserve analyticity, the integration path must be deformed so that the crossing does not actually take place. Equivalently, we can keep the main integration path on the imaginary axis and add integration contours around the poles that cross the imaginary axis. In the end, we obtain a path like the one of figure 4, where the thick poles are the moving ones. Finally, when we make the Wick rotation to the real axis, we obtain an integration path like the one shown in figure 5 or, depending on p, figure 6. In these pictures we have assumed for simplicity that the external space momentum $\mathbf{p}$ vanishes. The integration paths obtained from the Wick rotation agree with those prescribed by Lee and Wick. The general rule, valid for arbitrary Feynman diagrams, is that the left LW pair of a propagator is always above the integration path, while the right LW pair is always below.

When the right (respectively, left) LW pair of the propagator $D(k^2, m_1^2, \epsilon_1)$ hits the left (right) LW pair of $D((k-p)^2, m_2^2, \epsilon_2)$, the integration path gets pinched. We call this occurrence *LW pinching*.

The integration paths before and after the LW pinching are illustrated in figures 5 and 6. When we perform the Wick rotation, the analytic continuation is straightforward in the situation of figure 5, but we find an unexpected behavior in the situation of figure 6. The two situations correspond to disjoint regions $\mathcal{A}_1$ and $\mathcal{A}_2$ of the complex p^0 plane.

JHEP06(2017)066

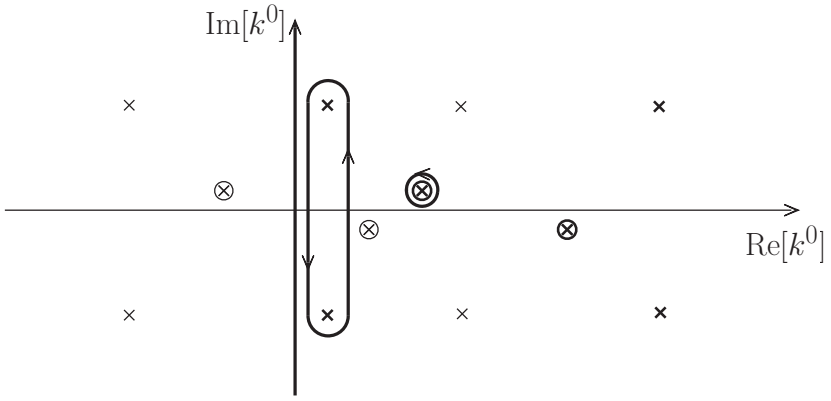

Figure 4. Euclidean integration path of the bubble diagram.

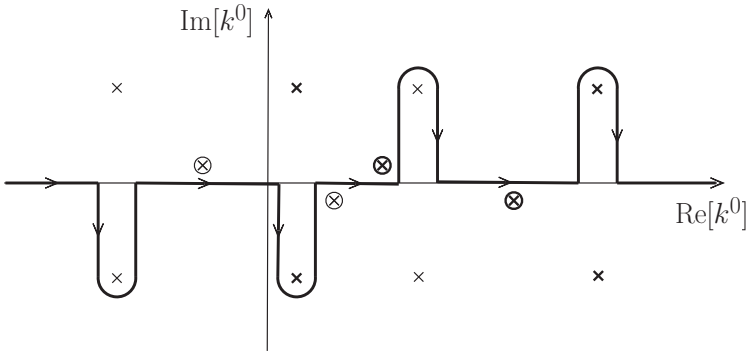

Figure 5. Integration path of the bubble diagram after the Wick rotation.

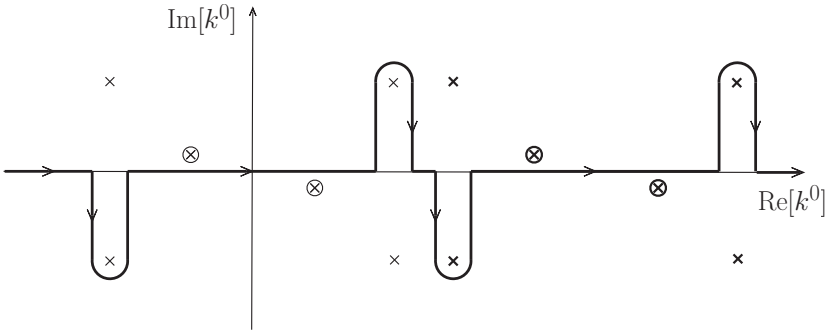

Figure 6. Integration path of the bubble diagram after the Wick rotation.

Each region $\mathcal{A}_i$ must be studied separately and gives a complex function $\mathcal{J}_i(p)$. The complex functions $\mathcal{J}_1(p)$ and $\mathcal{J}_2(p)$ are not related to each other by an analytic continuation. However they are still related in a well defined, nonanalytic way.

We show that, with these caveats, the procedure to handle the LW pinching is intrinsic to our definition of the theory, pretty much like the $i\epsilon$ prescription is intrinsic to the definition of a theory as a Wick rotated Euclidean one. Moreover, it is consistent with perturbative unitarity.

JHEP06(2017)066

The LW pinching motivated some authors to propose ad hoc prescriptions to handle it. The CLOP prescription [3], for example, amounts to deform the scale M in one of the propagators of the integral (2.3) to a different value M'. Under certain conditions, the pinching is absent for $M' \neq M$, the regions we mentioned above are analytically connected and the Wick rotation is analytic everywhere. After the calculation of the amplitude, the deformed scale M' is sent to M. This operation cuts the complex plane into disconnected regions.

The CLOP prescription is not sufficient to deal with the LW pinching in all the diagrams, because higher-order diagrams are expected to be ambiguous [3]. Moreover, it appears to be artificial. For example, there is no obvious way to incorporate it into the Lagrangian or the Feynman rules. In this paper, we also show that the CLOP prescription leads to physical predictions that differ from the ones we obtain and are ambiguous even in the case of the bubble diagram with $m_1 \neq m_2$. We also show that, if we strictly apply the rules that follow from the formulation of this paper, it is possible to retrieve the correct result even starting from $M' \neq M$ and letting M' tend to M at the end. Then, however, the CLOP prescription becomes redundant.

In section 6 we explain how the results of this section extend from the bubble diagram to more complicated diagrams.

To summarize, we show that the nonanalytically Wick rotated theory is well defined and intrinsically equipped with the procedure that allows us to handle the LW pinching. Instead, the prescriptions that can be found in the literature are ambiguous or redundant and give predictions that may be in contradiction with ours.

3 LW pinching

In this section we describe the LW pinching in the case of the bubble diagram (figure 3), that is to say the loop integral (2.3). First, we integrate on the loop energy k^0 by means of the residue theorem. This operation leaves us with the integral on the loop space momentum $\mathbf{k}$. Orienting the external space momentum $\mathbf{p}$ along the vertical line, the integral on the azimuth is trivial, so we remain with the integral on $k_s \equiv |\mathbf{k}|$ from 0 to ∞ and the integral on $u \equiv \cos\theta$ from -1 to 1, where θ is the zenith angle. To illustrate the problematics involved in the LW pinching exhaustively, we consider two cases. In the first case we work at $\mathbf{p} = 0$, in the second case we work at $\mathbf{p} \neq 0$. Lorentz invariance suggests that there should be no big difference between the two situations. It turns out that it is not so, because the method of calculation we are using is not manifestly Lorentz invariant. The calculation at $\mathbf{p} = 0$ misses some crucial points, which are visible only at $\mathbf{p} \neq 0$.

3.1 LW pinching at zero external space momentum

The LW pinching may involve pairs of LW poles (in which case it is called *pure* LW pinching) or one LW pole and a standard pole (in which case it is called *mixed* LW pinching). For the moment, we focus on the pure LW pinching, because at one loop the mixed one cannot occur for real external momenta.

There are two basic cases of pure LW pinching, shown in figure 7. The first case involves the right LW pair of the first propagator and the left LW pair of the second propagator.

JHEP06(2017)066

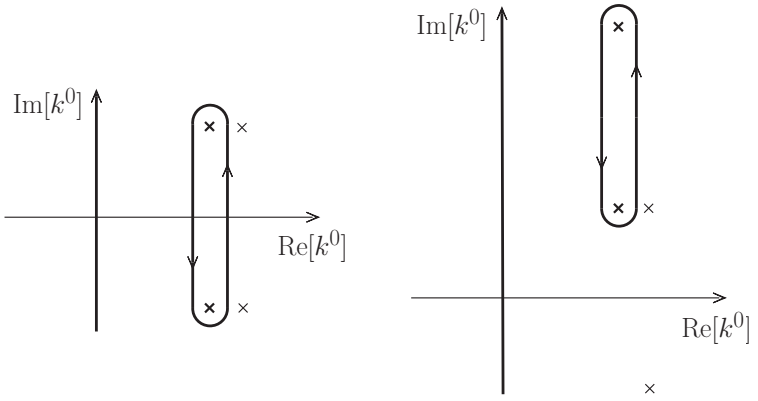

Figure 7. Lee-Wick pinching.

The second case involves the upper-right LW pole of the first propagator and the bottom-left LW pole of the second propagator. The other LW pinchings are the complex conjugates of the ones just described and their reflections with respect to the imaginary axis.

At $\mathbf{p} = 0$, there is no u dependence, so the u integral is trivial, the only nontrivial integration variable being k_s. The poles relevant to the top pinching occurring in the left figure 7 are

$$\frac{1}{k^0 - p^0 + \Omega_M^*(\mathbf{k})} \frac{1}{k^0 - \Omega_M(\mathbf{k})}, \tag{3.1}$$

while those relevant to the bottom pinching give the complex conjugate of this expression. The pinching occurs when k^0 is such that the locations of the two poles coincide, which gives the pinching equation

$$p^0 = \sqrt{k_s^2 + iM^2} + \sqrt{k_s^2 - iM^2}, \tag{3.2}$$

solved by

$$k_s^2 = \frac{(p^0)^4 - 4M^4}{4(p^0)^2}. \tag{3.3}$$

The poles relevant to the pinching occurring in the right figure 7 are

$$\frac{1}{k^0 - p^0 + \Omega_M(\mathbf{k})} \frac{1}{k^0 - \Omega_M(\mathbf{k})}.$$

They give the pinching equations

$$p^0 = 2\sqrt{k_s^2 + iM^2}, \tag{3.4}$$

which are solved by

$$k_s^2 = \frac{(p^0)^2}{4} - iM^2. \tag{3.5}$$

We denote the k_s integration path by Γ_k. By default, we expect it to be the positive real axis, but in a moment we will discover that we must deform it to include complex values.

When k_s is real and positive, the solution of (3.2) exists for p^2 real and larger than $2M^2$, while the solution of (3.4) exists when $p^2 - 4iM^2$ is real and larger than zero. Thus,

JHEP06(2017)066

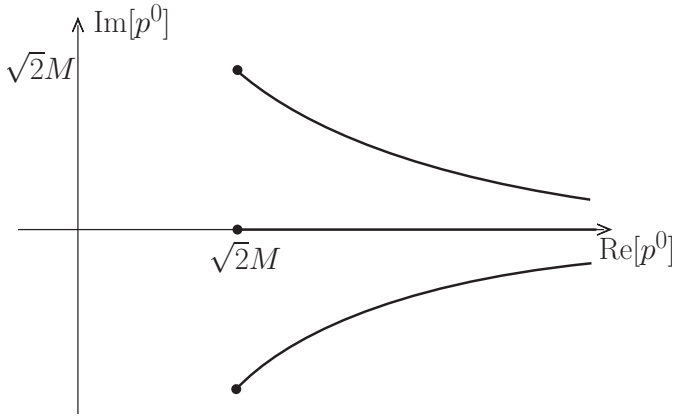

Figure 8. Branch cuts due to the Lee-Wick pinching at $\mathbf{p} = 0$.

the integral in $\mathcal{J}(p)$ has the LW branch cuts shown in figure 8 and symmetric ones with respect to the imaginary axis. The middle branch point corresponds to the *LW threshold* $p^2 = 2M^2$, while the other two branch points correspond to the LW thresholds $p^2 = 4iM^2$ and $p^2 = -4iM^2$. We have not shown the branch cuts associated with the standard pinching and the mixed LW pinching. When we vary p^0 across a branch cut of figure 8, a pole ν of the k_s integrand crosses the k_s integration path Γ_k (which means that the imaginary part of the pole becomes zero, while its real part stays positive), so the function $\mathcal{J}(p)$ is not analytic in that point.

For example, the right-hand side of (3.3) has vanishing imaginary part and positive real part for $x \geqslant \sqrt{2}M$, $y = 0$, where $x \equiv \mathrm{Re}[p^0]$, $y \equiv \mathrm{Im}[p^0]$. This gives the middle branch cut of figure 8, which starts from $p^0 = \sqrt{2}M$. A mirror branch cut is obtained by reflecting with respect to the imaginary axis.

On the other hand, the right-hand side of (3.5) has vanishing imaginary part and positive real part when

$$xy = 2M^2, \qquad x^2 \geqslant y^2. \tag{3.6}$$

This gives the branch cut shown in the first quadrant of figure 8, which starts from $p^0 = \sqrt{2}M(1+i)$, and a symmetric branch cut in the third quadrant. The complex conjugate LW pinching gives the branch cut shown in the fourth quadrant of figure 8, with branch point $p^0 = \sqrt{2}M(1-i)$, and a symmetric branch cut in the second quadrant.

So far, we have described what happens when Γ_k is not deformed. We have seen that in that case certain poles ν of the integrand cross Γ_k when p^0 crosses the cuts of figure 8. There, the function $\mathcal{J}(p)$ is not analytic. This is what we naturally obtain, for example, if we make the integration numerically, since a generic program of numerical integration does not know how to analytically deform the integration paths.

If we want to turn $\mathcal{J}(p)$ into a function that is analytic in a subdomain $\mathcal{O}$ that intersects the branch cuts of figure 8, we have to move those branch cuts away from $\mathcal{O}$. This is done by deforming Γ_k when the poles ν approach it, so as to prevent ν from crossing Γ_k in $\mathcal{O}$, and make the crossing occur at different values of p^0. Or, we can keep the integration path Γ_k rigid, but add or subtract (depending on the direction of motion of ν) the residues of

JHEP06(2017)066

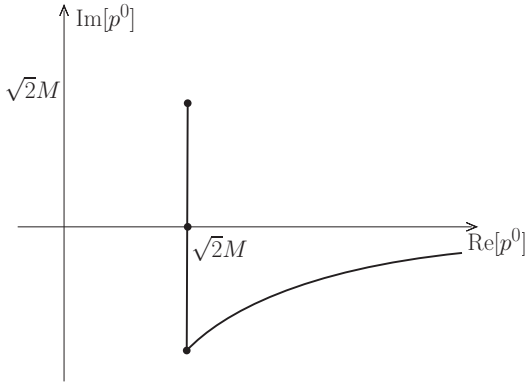

Figure 9. Analytic deformation of the branch cuts.

the moving poles ν after the crossing. For example, in the equal mass case $m_1 = m_2 = m$, it is easy to check that analyticity on the real axis above the LW threshold $p^2 = 2M^2$ is effectived restored by the replacement

$$\mathcal{J}(p) \to \mathcal{J}(p) - \frac{1}{16\pi}\frac{M^4}{m^4 + M^4}\sqrt{1 - \frac{4M^4}{(p^2)^2}}\theta_-(p^2 - 2M^2),$$

when p^0 crosses the real axis above $\sqrt{2}M$ from the upper half plane in the first quadrant (or below $-\sqrt{2}M$ from the lower half plane in the third quadrant), where $\theta_-(x) = 1$ for $\mathrm{Re}[x] > 0$, $\mathrm{Im}[x] < 0$ and $\theta_-(x) = 0$ in all other cases. In both sides of this replacement the integration path Γ_k is the positive real axis.

Deforming the cuts with this procedure, we may obtain, for example, figure 9. Now the amplitude $\mathcal{M}(p) = -i\lambda^2\mathcal{J}(p)/2$ is mathematically well defined on the real axis, but it has a nontrivial imaginary part for p^0 real and such that $(p^0)^2 > 2M^2$, which violates unitarity. To preserve unitarity, we must keep the branch cuts symmetric with respect to the real axis. At $\mathbf{p} = 0$ this implies that a branch cut is necessarily on the real axis, which makes the amplitude ill defined there.

3.2 LW pinching at nonzero external space momentum

At $\mathbf{p} \neq 0$ several interesting phenomena occur, which eventually lead to the solution of the problem of properly handling the LW pinching. The pinching equations (3.2) and (3.4) become

$$p^0 = \sqrt{\mathbf{k}^2 + iM^2} + \sqrt{(\mathbf{k} - \mathbf{p})^2 - iM^2}, \qquad p^0 = \sqrt{\mathbf{k}^2 + iM^2} + \sqrt{(\mathbf{k} - \mathbf{p})^2 + iM^2}, \quad (3.7)$$

respectively, plus their complex conjugates. Keeping $\mathbf{p}$ fixed, the solutions fill extended surfaces, shown in figure 10. The first picture is obtained for smaller values of $|\mathbf{p}|$, the second picture for larger values.

Since the right-hand sides of (3.7) now depend on two parameters, k_s and u, the lines of figure 8 have enlarged into regions $\tilde{\mathcal{A}}_i$ of nonvanishing measure. Let $\tilde{\mathcal{A}}_0$ denote the region that contains the imaginary axis, which we call *main region*, and $\tilde{\mathcal{A}}_P$ the one that

JHEP06(2017)066

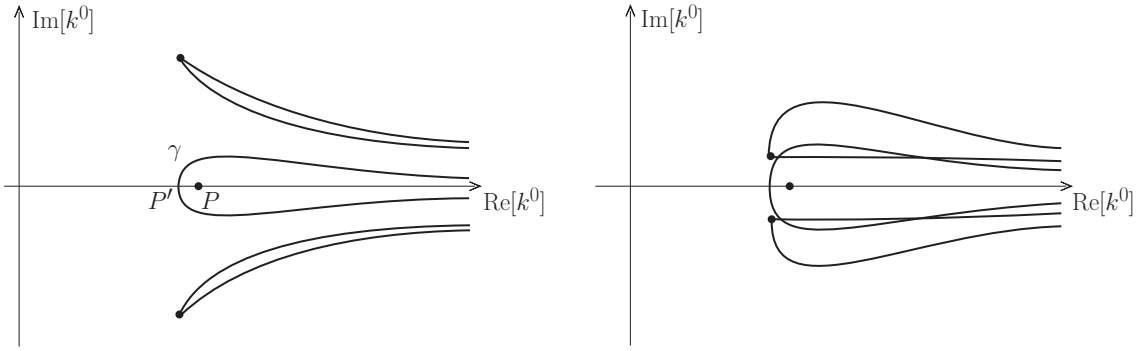

Figure 10. Solutions of the Lee-Wick pinching conditions at $\mathbf{p} \neq 0$.

contains the point P, located at $p^0 = \sqrt{2M^2 + \mathbf{p}^2} \equiv E_P$. Such a point corresponds to the LW threshold $p^2 = 2M^2$. Finally, we call $\tilde{\mathcal{A}}'_P$ the region symmetric to $\tilde{\mathcal{A}}_P$ with respect to the imaginary axis. The regions $\tilde{\mathcal{A}}_i$ other than $\tilde{\mathcal{A}}_0$ collect the values of p^0 that satisfy the equations (3.7) for real $\mathbf{k}$. There, $\mathcal{J}(p)$ gives nonanalytic, Lorentz violating results, if the $\mathbf{k}$ integral is performed on its natural, real domain. Now we give details on these issues and later explain how Lorentz invariance and analyticity are recovered.

The curve γ is the boundary of the region $\tilde{\mathcal{A}}_P$. It does not cross the real axis in P, but in the point P', which has energy

$$p^0 = \sqrt{\frac{\mathbf{p}^2}{2} + \sqrt{\frac{(\mathbf{p}^2)^2}{4} + 4M^4}} \equiv E_{P'} \tag{3.8}$$

and satisfies $\sqrt{2}M < E_{P'} < E_P$. Clearly, Lorentz invariance is violated, because P' and γ have no Lorentz invariant meaning. This fact has been noticed by Nakanishi in ref. [11]. The intuitive reason is that, as shown in figure 2, the loop energy is not everywhere real, so, if we want Lorentz invariance, the loop momentum cannot be everywhere real. Said differently, if we want to restore Lorentz invariance working at $\mathbf{p} \neq 0$, we must deform the $\mathbf{k}$ integration domain to include complex values, till the regions $\tilde{\mathcal{A}}_i$ are squeezed back to Lorentz invariant lines (i.e. solutions of Lorentz invariant conditions), like those of figure 8. In particular, the region $\tilde{\mathcal{A}}_P$ must be turned into the half line $\mathcal{O}_P$ that corresponds to p^0 real located above the LW threshold, i.e. $p^0 \geqslant E_P$. During the deformation process we can keep the deformed figure 10 symmetric with respect to the real axis. To achieve this goal, it is sufficient to separate the contributions of the poles of each LW pair and deform the $\mathbf{k}$ integration domains in complex conjugate ways in the two cases.

Below we also show that when Lorentz invariance is violated (restored), analyticity is also violated (restored).

3.3 Lorentz invariance and analyticity above the LW threshold

Now we study the amplitude in $\mathcal{O}_P$, its Lorentz invariance and analyticity. It is convenient to separate the contributions of the physical poles from the ones of the LW poles by writing the propagator (2.1) as

$$iD_0(p^2, m^2, \epsilon) + iD_{\rm LW}(p^2, m^2), \tag{3.9}$$

JHEP06(2017)066

where

$$D_0(p^2, m^2, \epsilon) = \frac{M^4}{M^4 + m^4} \frac{1}{p^2 - m^2 + i\epsilon}, \qquad D_{\rm LW}(p^2, m^2) = -\frac{M^4}{M^4 + m^4} \frac{p^2 + m^2}{(p^2)^2 + M^4}.$$

To simplify these expressions, we have replaced $m^2 - i\epsilon$ with m^2 where allowed.

We just need to focus on the contribution

$$\mathcal{J}_{\rm LW}(p) = \int \frac{{\rm d}^D k}{(2\pi)^D} D_{\rm LW}(k^2, m_1^2) D_{\rm LW}((k-p)^2, m_2^2) \tag{3.10}$$

to the bubble loop integral $\mathcal{J}(p)$, because for p real it is the only one interested by the LW pinching. Every other contribution admits an analytic Wick rotation.

We integrate on k^0 by means of the residue theorem, as usual, and assume that $\mathbf{k}$ is integrated on its natural real domain. Then, the function $\mathcal{J}_{\rm LW}(p)$ is analytic and Lorentz invariant in the main region $\tilde{\mathcal{A}}_0$, because the Wick rotation is analytic there. It is neither analytic nor Lorentz invariant inside $\tilde{\mathcal{A}}_P$. Nevertheless, in the next section we prove that $\mathcal{J}_{\rm LW}(p)$ is continuous everywhere if $\mathbf{p} \neq 0$. We denote the function $\mathcal{J}_{\rm LW}(p)$ restricted to $\tilde{\mathcal{A}}_0$ by $\mathcal{J}^0_{\rm LW}(p)$ and the same function restricted to $\tilde{\mathcal{A}}_P$ by $\mathcal{J}^P_{\rm LW}(p)$.

When we deform the $\mathbf{k}$ integration domain, $\mathcal{J}_{\rm LW}(p)$ changes into some new function $\mathcal{J}^{\rm def}_{\rm LW}(p)$, which depends on the deformation. Denote the deformed regions $\tilde{\mathcal{A}}_0$ and $\tilde{\mathcal{A}}_P$ by $\tilde{\mathcal{A}}^{\rm def}_0$ and $\tilde{\mathcal{A}}^{\rm def}_P$, respectively.

The function $\mathcal{J}^{\rm def}_{\rm LW}(p)$ is analytic in $\tilde{\mathcal{A}}^{\rm def}_0$ and coincides with $\mathcal{J}^0_{\rm LW}(p)$ in $\tilde{\mathcal{A}}_0 \cap \tilde{\mathcal{A}}^{\rm def}_0$. Moreover, as shown in the next section, it is continuous everywhere. When the domain deformation is finalized, i.e. the surfaces of figure 10 are turned into the desired lines (in particular, $\tilde{\mathcal{A}}_P$ is squeezed onto $\mathcal{O}_P$), $\mathcal{J}^{\rm def}_{\rm LW}(p)$ gives the final outcome to be assigned to the integral (3.10) in $\mathcal{O}_P$, which we denote by $\mathcal{J}^{>}_{\rm LW}(p)$.

We argue that

$$\mathcal{J}^{>}_{\rm LW}(p) = \frac{1}{2}\left[\mathcal{J}^{0+}_{\rm LW}(p) + \mathcal{J}^{0-}_{\rm LW}(p)\right], \tag{3.11}$$

where the functions $\mathcal{J}^{0\pm}_{\rm LW}(p)$ are defined as follows. Start from the function $\mathcal{J}^0_{\rm LW}(p)$ in $\tilde{\mathcal{A}}_0$, which we know to be analytic. We can analytically continue $\mathcal{J}^0_{\rm LW}(p)$ to $\mathcal{O}_P$ either from the half plane ${\rm Im}[p^0] > 0$ or from the half plane ${\rm Im}[p^0] < 0$, as shown in figure 11. These two possibilities give $\mathcal{J}^{0+}_{\rm LW}(p)$ and $\mathcal{J}^{0-}_{\rm LW}(p)$, respectively.

A number of arguments and checks, which we collect in the next section and in section 6, suggest that formula (3.11) is correct for every diagram. Alternatively, we can take the right-hand side of (3.11) as the very *definition* of $\mathcal{J}^{>}_{\rm LW}(p)$, bypassing the domain deformation described in the previous subsection.

The continuations that define $\mathcal{J}^{0\pm}_{\rm LW}(p)$ in $\mathcal{O}_P$ can be stretched to neighborhoods of $\mathcal{O}_P$ above P, so both functions $\mathcal{J}^{0\pm}_{\rm LW}(p)$ are analytic in such neighborhoods. Moreover, they are Lorentz invariant, because they are obtained from $\mathcal{J}^0_{\rm LW}(p)$, which is Lorentz invariant. Thus, formula (3.11) ensures that $\mathcal{J}^{>}_{\rm LW}(p)$ is analytic and Lorentz invariant in a neighborhood of the real axis above the LW threshold.

The function $\mathcal{J}_{\rm LW}(p)$ is purely imaginary on the real axis, because the integrand and the $\mathbf{k}$ integration domain are real. Indeed, when we apply the residue theorem to integrate on

JHEP06(2017)066

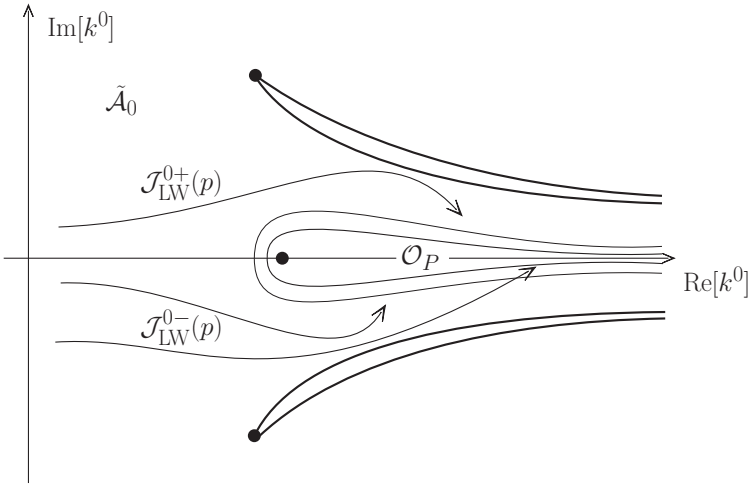

Figure 11. Definitions of $\mathcal{J}^{0+}_{\rm LW}(p)$ and $\mathcal{J}^{0-}_{\rm LW}(p)$.

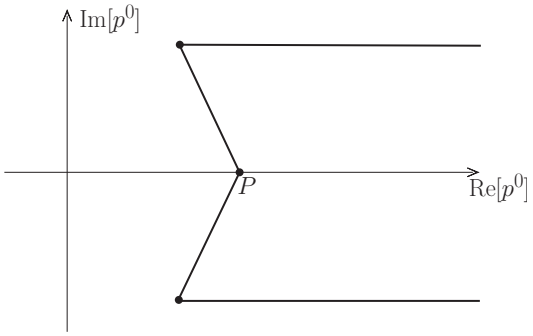

Figure 12. Final analytic regions $\mathcal{A}_i$.

k^0, we pick pairs of complex conjugate poles and get an overall factor i. Thus, $\mathcal{J}^0_{\rm LW}(p) = -[\mathcal{J}^0_{\rm LW}(p^*)]^*$, which implies $\mathcal{J}^{0-}_{\rm LW}(p) = -[\mathcal{J}^{0+}_{\rm LW}(p^*)]^*$. Since the contributions due to the poles of each LW pair are interested by complex conjugate deformations of the respective $\mathbf{k}$ integration domains, $\mathcal{J}^{\rm def}_{\rm LW}(p)$ obeys similar relations thoughout the deformation. Then, $\mathcal{J}^{>}_{\rm LW}(p)$ is purely imaginary in $\mathcal{O}_P$ and so is the right-hand side of (3.11). The amplitude $\mathcal{M}(p) = -i\lambda^2\mathcal{J}(p)/2$ satisfies unitarity, because the LW contributions do not affect its imaginary part on the real axis. More details about unitarity can be found in ref. [23].

It may be helpful to analytically continue the result from the mentioned neighborhoods to larger regions. Focusing on the three regions that have nontrivial intersections with the real axis, in the end we may get, for example, a final figure like figure 12 plus its symmetrization with respect to the imaginary axis. We see that the complex plane is divided into the disjoint regions $\mathcal{A}_0$, $\mathcal{A}_P$ and $\mathcal{A}'_P$, which are originated by the initial regions $\tilde{\mathcal{A}}_0$, $\tilde{\mathcal{A}}_P$ and $\tilde{\mathcal{A}}'_P$ through the deformation process described previously.

Note that formula (3.11) allows us to find $\mathcal{J}^{>}_{\rm LW}(p)$ without effectively going through the domain deformation process (which is practically hard to implement): it is sufficient to decompose the propagators as in formula (3.9), isolate the contributions interested by

JHEP06(2017)066

the LW pinching, analytically continue them from the main region $\tilde{\mathcal{A}}_0$ to $\mathcal{O}_P$ in the two possible ways and finally average the results. As said, formula (3.11) could also be taken as the definition of the function $\mathcal{J}^{>}_{\rm LW}(p)$ in $\mathcal{O}_P$.

To summarize, the integral $\mathcal{J}(p)$ is ill defined at $\mathbf{p} = 0$, but it can be worked out from $\mathbf{p} \neq 0$, without the need of ad hoc prescriptions. We have derived the results in the case of the bubble diagram, but the specificity of that diagram never really enters, so we expect that the conclusions hold for every diagram. More comments on this are contained in section 6. An explicit check of the result (3.11) is given in the next section [see the comments around formula (4.9)].

4 Calculation around the LW pinching

In this section we illustrate the calculations in the presence of the LW pinching, prove the continuity of $\mathcal{J}_{\rm LW}(p)$ and $\mathcal{J}^{\rm def}_{\rm LW}(p)$ and provide arguments and checks in favor of formula (3.11). For definiteness, we assume to work in more than two spacetime dimensions.

We focus on the pinching depicted in the left figure 7. The $\mathbf{k}$ integral has potential singularities of the form $1/D_0$ and $1/D_0^*$, where

$$D_0 = p^0 - \Omega_M(\mathbf{k}) - \Omega_M^*(\mathbf{k} - \mathbf{p}). \tag{4.1}$$

The top pinching occurs for $D_0 = 0$, i.e.

$$p^0 = \sqrt{\mathbf{k}^2 + iM^2} + \sqrt{(\mathbf{k} - \mathbf{p})^2 - iM^2}, \tag{4.2}$$

while the bottom pinching occurs for $D_0^* = 0$. The conditions are complex for $\mathbf{p} \neq 0$, so they split into two real conditions.

We want to study $\mathcal{J}(p)$ above the LW threshold, so we take a real $p^0 > \sqrt{\mathbf{p}^2 + 2M^2}$. With a real loop space momentum $\mathbf{k}$, the solution of (4.2) is a circle, equal to the intersection between a sphere and a plane, given by

$$\mathbf{k}^2 = \frac{(p^0)^4 - 4M^4}{4(p^0)^2}, \qquad \mathbf{p}^2 = 2\mathbf{p} \cdot \mathbf{k}. \tag{4.3}$$

If the external energy p^0 is complex, the analysis becomes more involved, but for our purposes it is sufficient to focus on the values of p^0 that are close to the real axis. This can be achieved by making the substitution $p^0 \to p^0 \mathrm{e}^{i\varphi}$, with φ small, after which we can keep p^0 real. The denominator becomes

$$D_\varphi = p^0 \mathrm{e}^{i\varphi} - \Omega_M(\mathbf{k}) - \Omega_M^*(\mathbf{k} - \mathbf{p}).$$

To simplify the formulas, we expand D_φ around the solution (4.3) by means of the change of variables

$$k_s = \frac{\sigma_-}{2p^0} + \tau \frac{\sigma_+^2}{2\sigma_-(p^0)^2} + \eta \frac{p_s \sigma_+^2}{4\sigma_- M^2}, \qquad u = \frac{p_s}{2k_s} + \eta \frac{\sigma_+^2}{2\sigma_- M^2}, \tag{4.4}$$

JHEP06(2017)066

where $\sigma_\pm \equiv \sqrt{(p^0)^4 \pm 4M^4}$, $p_s \equiv |\mathbf{p}|$ and $u = \cos\theta$, θ being the angle between the vectors $\mathbf{p}$ and $\mathbf{k}$. The fluctuations around the solutions (4.3) are parametrized by τ and η. The integrand of $\mathcal{J}(p)$ is proportional to

$$\frac{\mathrm{d}^{D-1}\mathbf{k}}{D_\varphi} \to -\frac{2\pi^{(D-2)/2}}{\Gamma\left(\frac{D}{2}-1\right)} \frac{k_s^{D-2}(1-u^2)^{(D-4)/2}\mathrm{d}k_s\mathrm{d}u}{\tau - i(p^0\varphi + p_s\eta)}, \tag{4.5}$$

where the arrow means that we have integrated on all the angles besides θ. We have also expanded the denominator to the first order in φ, τ and η.

We see that as long as either φ or p_s are different from zero, the potential singularity at $D_\varphi = 0$ is integrable. In particular, if we keep $p_s \neq 0$ and reach $\varphi = 0$, we obtain

$$\frac{\mathrm{d}^{D-1}\mathbf{k}}{D_0} \to -\frac{2\pi^{(D-2)/2}}{\Gamma\left(\frac{D}{2}-1\right)} \frac{\sigma_+^4\sigma_-^{D-4}}{(2p^0)^D M^2}(1-u^2)^{(D-4)/2}\frac{\mathrm{d}\tau\mathrm{d}\eta}{\tau - ip_s\eta}. \tag{4.6}$$

It is interesting to study the limit $p_s \to 0$ of this expression, which gives

$$-\frac{4\pi^{(D-2)/2}}{\Gamma\left(\frac{D}{2}-1\right)} \frac{\sigma_+^2\sigma_-^{D-3}}{(2p^0)^D}(1-u^2)^{(D-4)/2}\mathrm{d}\tau\mathrm{d}u\left[\mathcal{P}\left(\frac{1}{\tau}\right) + i\pi\,\mathrm{sgn}(u)\delta(\tau)\right], \tag{4.7}$$

where $\mathcal{P}$ denotes the principal value and sgn is the sign function. We learn that in this case p_s provides the prescription for handling the integral. Note that at $p_s = 0$ no u dependence survives in the integrand, besides the sign function of formula (4.7) and the factor $(1-u^2)^{(D-4)/2}$ coming from the integration measure. If we perform the simple u integration, we finally get

$$-\frac{4\pi^{(D-1)/2}}{\Gamma\left(\frac{D-1}{2}\right)} \frac{\sigma_+^2\sigma_-^{D-3}}{(2p^0)^D}\mathrm{d}\tau\mathcal{P}\left(\frac{1}{\tau}\right). \tag{4.8}$$

Also note that in three and higher dimensions there is no singularity for $\sigma_- \to 0^+$.

Formula (4.6), applied to $\mathcal{J}_{\mathrm{LW}}(p)$ at $p_s \neq 0$, shows that $\mathcal{J}_{\mathrm{LW}}(p)$ is continuous everywhere on the complex p^0 plane, as anticipated in the previous section. We have also checked the continuity of $\mathcal{J}_{\mathrm{LW}}(p)$ numerically, by means of a computer program.

If we use formula (4.8) in $\mathcal{J}_{\mathrm{LW}}(p)$, we can work out the function $\mathcal{J}^{>}_{\mathrm{LW}}(p)$ for $p_s \to 0$. Indeed, having set $\varphi = 0$ we have placed ourselves in $\mathcal{O}_P \subset \tilde{\mathcal{A}}_P$. This allows us to evaluate the integral $\mathcal{J}_{\mathrm{LW}}(p)$ there at $p_s \neq 0$. Then, the limit $p_s \to 0$ squeezes the region $\tilde{\mathcal{A}}_P$ onto $\mathcal{O}_P$ and so gives $\mathcal{J}^{>}_{\mathrm{LW}}(p)$. Here, it is unnecessary to actually perform the domain deformation, because the limit $p_s \to 0$ provides an equivalent effect.

Nowe we can check formula (3.11), proceeding as follows. We study the singularity $1/D_\varphi$ again, but first set $p_s = 0$ at nonzero φ and then send φ to zero. By formula (4.5), the denominator $\tau - ip_s\eta$ of (4.6) is replaced by $\tau - ip^0\varphi$, so, after integrating on u, we find

$$-\frac{4\pi^{(D-1)/2}}{\Gamma\left(\frac{D-1}{2}\right)} \frac{\sigma_+^2\sigma_-^{D-3}}{(2p^0)^D}\frac{\mathrm{d}\tau}{\tau - ip^0\varphi} \underset{\varphi\to 0^\pm}{\longrightarrow} -\frac{4\pi^{(D-1)/2}}{\Gamma\left(\frac{D-1}{2}\right)} \frac{\sigma_+^2\sigma_-^{D-3}}{(2p^0)^D}\mathrm{d}\tau\left[\mathcal{P}\left(\frac{1}{\tau}\right) \pm i\pi\delta(\tau)\right]. \tag{4.9}$$

These expressions are also regular, but do not coincide with (4.8).

JHEP06(2017)066

Observe that the result (4.9) is obtained by first squeezing the region $\tilde{\mathcal{A}}_P$ onto $\mathcal{O}_P$ (which is a consequence of letting $p_s \to 0$ first) and then approaching the real axis from $\mathrm{Im}[p^0] > 0$ ($\varphi \to 0^+$) or $\mathrm{Im}[p^0] < 0$ ($\varphi \to 0^-$). The two cases give $\mathcal{J}^{0+}_{\rm LW}(p)$ and $\mathcal{J}^{0-}_{\rm LW}(p)$, respectively. If we average the two results (4.9), we obtain (4.8), in agreement with formula (3.11).

We expect that the key results just found continue to hold through the domain deformation that defines the amplitude in $\mathcal{O}_P$ at $\mathbf{p} \neq 0$. For example, the basic reason why $\mathcal{J}_{\rm LW}(p)$ is continuous everywhere is that the denominator D_φ is complex, which makes the singularity integrable. However, the denominator remains complex during the domain deformation, so $\mathcal{J}^{\rm def}_{\rm LW}(p)$ is also continuous. Moreover, the check of formula (4.2) provided above, which works at $p_s \to 0$, captures the essential features that also apply at $\mathbf{p} \neq 0$, when the domain deformation is taken into account. Indeed, assume that the deformed region $\tilde{\mathcal{A}}^{\rm def}_P$ is a thin strip around $\mathcal{O}_P$. Let $\tilde{p}_s$ denote the length of the short edge of the strip, so that the domain deformation is finalized ($\tilde{\mathcal{A}}^{\rm def}_P \to \mathcal{O}_P$) when $\tilde{p}_s \to 0$. On general grounds, the potential singularity of the integral is always expected to be of the form

$$\sim \frac{\mathrm{d}\tau \mathrm{d}\eta}{\tau - i(p^0\varphi + \tilde{p}_s\eta)}, \tag{4.10}$$

where the external momentum is still written as $p^0 \mathrm{e}^{i\varphi}$, with p^0 real and φ small, while τ and η are two real variables that parametrize the fluctuations around the singular point at $\varphi = 0$ (τ being parallel to the long edge of the strip and η being parallel to the short edge). Repeating the arguments above with the help of (4.10), we still get formula (3.11).

The results just derived and formula (3.11) are expected to apply to the LW pinching of any diagram, because they are not tied to the peculiarities to the bubble diagram. See section 6 for more details on this.

4.1 Comparison with the CLOP and other prescriptions

We have seen that the theory is intrinsically equipped with the right recipe to handle the LW pinching. This means that any artificial prescription can potentially lead to wrong results. Now we classify the whole set of unitary prescriptions, which includes the CLOP one, and compare them with the results predicted by the formulation of this paper. For definiteness, we work in four dimensions.

Consider the integrand of the loop integral (2.3) at $\mathbf{p} = 0$. We begin with the top pinching that appears in the left figure 7, which is due to the poles (3.1). By means of the expansion

$$k_s = \frac{\sigma_-}{2p^0} + \tau \frac{Mp^0}{\sigma_-}, \tag{4.11}$$

we see that the integrand of $\mathcal{J}(p)$ behaves as

$$\frac{i}{(8\pi)^2} \frac{\sigma_-}{(p^0)^2} \frac{M^4}{(M^2 + im_1^2)(M^2 - im_2^2)} \frac{\mathrm{d}\tau}{\tau} \tag{4.12}$$

around the singularity $\tau = 0$.

JHEP06(2017)066

We know that the formulation of this paper removes the singularity because, working at nonvanishing $\mathbf{p}$ and letting $\mathbf{p}$ tend to zero afterwards, (4.12) is replaced by

$$\frac{i}{(8\pi)^2}\frac{\sigma_-}{(p^0)^2}\frac{M^4}{(M^2+im_1^2)(M^2-im_2^2)}\mathcal{P}\left(\frac{1}{\tau}\right)\mathrm{d}\tau. \tag{4.13}$$

More generally, we may have

$$\frac{i}{(8\pi)^2}\frac{\sigma_-}{(p^0)^2}\frac{M^4}{(M^2+im_1^2)(M^2-im_2^2)}\left[\mathcal{P}\left(\frac{1}{\tau}\right)+ia\delta(\tau)\right]\mathrm{d}\tau, \tag{4.14}$$

where a is an arbitrary real constant.

The LW poles come in conjugate pairs, so the pinching just considered is accompanied by the complex conjugate one, which occurs when the residue calculated in $k^0=p^0-\Omega_M(\mathbf{k})$ hits the LW pole located in $k^0=\Omega_M^*(\mathbf{k})$. The contribution is minus the complex conjugate of (4.14), because the i factor that accompanies the residue does not get conjugated. The total gives

$$\frac{2i}{(8\pi)^2}\frac{\sigma_-}{(p^0)^2}\frac{M^4}{(M^4+m_1^4)(M^4+m_2^4)}\left[(M^4+m_1^2m_2^2)\mathcal{P}\left(\frac{1}{\tau}\right)+aM^2(m_1^2-m_2^2)\delta(\tau)\right]\mathrm{d}\tau.$$

Again, the contribution to $\mathcal{J}(p)$ is regular and purely imaginary. In particular, it does not affect the imaginary part of the amplitude $\mathcal{M}(p)=-i\lambda^2\mathcal{J}(p)/2$. This result proves that the prescription (4.14) is consistent with perturbative unitarity for arbitrary a. However, the loop integral $\mathcal{J}(p)$ does depend on a, at least when the two physical masses are different. This proves that no prescription with nonvanishing a is consistent with our formulation, which predicts $a=0$.

The CLOP prescription is ambiguous and gives $a=\pm\pi$. This result can be proved by replacing the LW scale M with $M'=M+\delta$ in the second propagator of (2.3). Modifying the expansion (4.11) into

$$k_s=\frac{\sigma_-}{2p^0}+\tau\frac{Mp^0}{\sigma_-}-2\delta\frac{M^3}{p^0\sigma_-},$$

the integrand $\mathcal{J}(p)$ behaves as

$$\frac{i}{(8\pi)^2}\frac{\sigma_-}{(p^0)^2}\frac{iM^4}{(M^2+im_1^2)(M^2-im_2^2)}\frac{\mathrm{d}\tau}{\tau-i\delta}, \tag{4.15}$$

around the top pinching of the left figure 7. This formula is equivalent to (4.14) with $a=\pi\mathrm{sgn}(M'-M)$.

The result is ambiguous, because it depends on whether δ is chosen to be positive or negative and there is no way to decide whether M' must be smaller than M or the contrary. In the next section we plot the ambiguity numerically.

Before this result, ambiguities due to the CLOP prescription were expected only in more complicated diagrams [3]. It was understood that maybe it was possible to resolve them by means of further prescriptions. The ambiguity we have just found is present already at one loop and in one of the simplest Feynman diagrams. However, it occurs only when $m_1\neq m_2$, which explains why it was not noticed before. For example, the results

JHEP06(2017)066

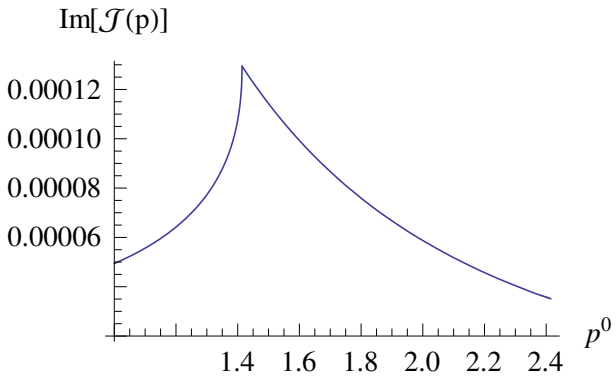

Figure 13. Plot of $\mathrm{Im}[\mathcal{J}(p)]$ around the LW pinching.

of ref. [12] are correct, since they are made in the case $m_1 = m_2 = m$, where the CLOP prescription gives the same result as our formulation.

If we want to make the new ambiguity disappear, we can supplement the CLOP prescription by an average over the two possibilities $a = \pm\pi$, which effectively gives $a = 0$ and agrees with our result (4.13). This makes the amended prescription even more artificial than the original CLOP approach and there is still no guarantee that analogous way outs can be found in more complicated situations. For these reasons, we think that ad hoc approaches like the CLOP one should be dropped in favor of the new formulation of this paper, which does not have such problems.

5 Complete bubble diagram

In this section, we complete the calculation of the bubble diagram. The main goal is to describe what happens around the LW threshold. Since the threshold associated with the physical poles is not the main focus of the calculation, we avoid the superposition between the physical threshold and the LW one by assuming that the masses m_1 and m_2 are sufficiently large. For concreteness, we take $m_1, m_2 \geqslant 3M$.

Another simplifying choice is to make the calculation at $\mathbf{p} = 0$ and resolve the singularity with the help of formula (4.8). We know that this procedure is justified by starting from nonvanishing $\mathbf{p}$, where the LW pinching is properly handled, and taking the limit $\mathbf{p} \to 0$ afterwards.

Setting $M = 1$ and $m_1 = m_2 = 3$, the imaginary part of $\mathcal{J}(p)$ as a function of a real p^0 has the behavior of figure 13. The real part vanishes in the range shown, in agreement with unitarity. We see that the imaginary part is well defined and continuous, but not analytic. The nonanalyticity that is visible at $p^2 = 2M^2$ is the remnant of the LW pinching. If in nature some physical processes are described by a LW theory, the LW scale M is the key physical quantity signaling the new physics. A shape like the one of figure 13 may be helpful to determine the magnitude of M experimentally.

The formulation of the theory by nonanalytically Wick rotating its Euclidean version gives an unambiguous answer and does not need ad hoc prescriptions. The CLOP pre-

JHEP06(2017)066

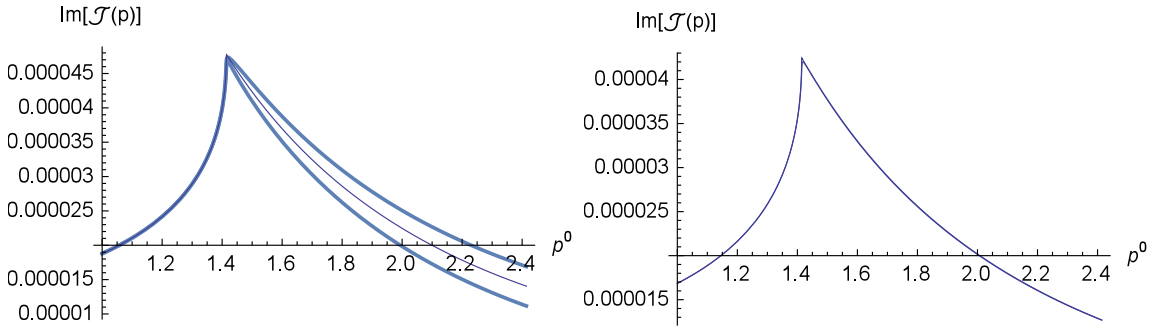

Figure 14. Comparison between our formulation and the CLOP prescription.

scription gives the same result, in the case just considered. As explained in the previous section, we can appreciate the intrinsic ambiguity of the CLOP prescription and the differences with the predictions of our formulation by studying the bubble diagram with unequal masses. For example, we compare the case $m_1 = 3$, $m_2 = 5$ to the case $m_1 = m_2 = 4$.

Using the CLOP prescription, we take $M = 1$ in the first propagator of formula (2.3) and $M = 1 + \delta$ in the second propagator, working at $\mathbf{p} = 0$. Then we integrate $\mathcal{J}(p)$ numerically for smaller and smaller values of $|\delta|$, till, say, $|\delta| = 10^{-3}$. We study both $\delta = -10^{-3}$ and $\delta = 10^{-3}$.

On the other hand, following the formulation proposed here, we set $M = 1$ in both propagators, but keep $p_s = |\mathbf{p}|$ different from zero. Then, we integrate numerically for smaller and smaller values of p_s till $p_s = 10^{-3}$.

Collecting the results of these calculations, the imaginary part of $\mathcal{J}(p)$ gives the plots of figure 14, while the real part still vanishes. The first plot refers to the case $m_1 = 3$, $m_2 = 5$, while the second plot refers to the case $m_1 = m_2 = 4$. Let us describe the first plot in detail. Below the LW threshold, the graph is unique, which means that our formulation and the CLOP prescription give the same result. Above the LW threshold, we see three graphs. The middle graph is the one predicted by our formulation, while the upper and lower graphs are those predicted by the CLOP prescription, with $\delta = -10^{-3}$ and $\delta = 10^{-3}$, respectively.

Although the match is very precise in the equal mass case (second figure), there is a remarkable discrepancy above the LW threshold in the unequal mass case. These results confirm that the CLOP prescription gives two different results depending on whether $M' > M$ or $M' < M$. The average of the two CLOP graphs coincides with the graph predicted by our formulation.

If we really want to retrieve our result from a procedure where the propagators of formula (2.3) have two different LW scales M and M', as in the CLOP prescription, we actually can, but in that case the CLOP prescription becomes redundant. Instead of setting $p_s = 0$ and then letting M' tend to M, we must start from $p_s \neq 0$, let M' approach M while $p_s \neq 0$, work in a suitable region $\tilde{\mathcal{A}}_>$, perform the domain deformation and only at the end, if we want, let p_s tend to zero.

In more detail, the region $\tilde{\mathcal{A}}_P$ contained in the curve γ of figure 10 splits into two regions $\tilde{\mathcal{A}}_P^+$ and $\tilde{\mathcal{A}}_P^-$, when $M' = 1 + \delta$ is sufficiently different from M (or p_s is sufficiently

JHEP06(2017)066

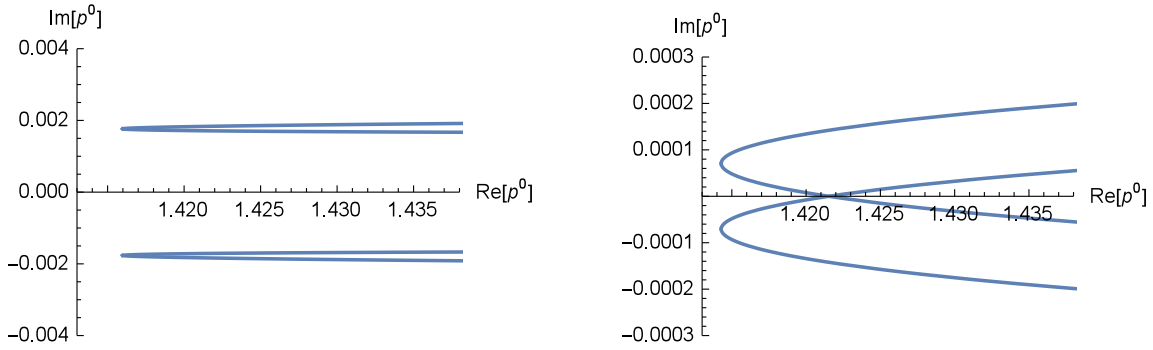

Figure 15. Areas of LW pinching when $M' \neq M$.

large). We show the new regions in figure 15, where we have taken $p_s = 10^{-3}$ and $M = 1$. In the left picture $\delta = 5 \cdot 10^{-3}$, while in the right picture $\delta = 10^{-4}$.

When δ is sufficiently large, the real axis has no intersection with $\tilde{\mathcal{A}}_P^+$ and $\tilde{\mathcal{A}}_P^-$, but when δ becomes smaller, the region $\tilde{\mathcal{A}}_> \equiv \tilde{\mathcal{A}}_P^+ \cap \tilde{\mathcal{A}}_P^-$ is nonempty. What the CLOP prescription requires is to cover the entire real axis by analytic continuation from below (i.e. from the region that contains the imaginary axis) and let δ tend to zero at the end. What our formulation requires, instead, is to reach the portion of the real axis that is located above the LW threshold P by working in $\tilde{\mathcal{A}}_>$, perform the domain deformation that squeezes $\tilde{\mathcal{A}}_>$ onto the real axis, let δ tend to zero and finally analytically continue the result to reach P from above. This is the crucial difference between the two formulations, which explains the discrepancy shown in figure 14.

6 More complicated diagrams

In this section, we explain how the arguments of the previous sections can be extended to more complicated diagrams. One-loop diagrams have a unique loop momentum, while the independent external momenta can be arbitrarily many. The pure LW pinchings are similar to the ones of the bubble diagram. They occur between the right LW poles of any propagator and the left LW poles of any other propagator, as described by figure 6. The mixed LW pinching cannot occur for real external momenta.

At higher loops the pinching is also analogous to the one we are accustomed to in common theories. There, if the propagators of the internal legs of the diagram have masses m_i, the pinchings lead to thresholds of the form $p^2 = (m_{i_1} + m_{i_2} + m_{i_3} + \cdots)^2$, where p is a sum of incoming momenta. In the case of the LW pinching, the formulas that give the thresholds are basically the same, with the difference that some masses m_i are replaced by the complex masses $M_\pm = (1 \pm i)M/\sqrt{2}$ associated with the LW scales. The pinching conditions are always of the form $p^0 =$ positive sum of (possibly complex) frequencies and the thresholds are

$$p^2 = \left[(n_+ + n_-)\frac{M}{\sqrt{2}} + i(n_+ - n_-)\frac{M}{\sqrt{2}} + m_{i_1} + m_{i_2} + m_{i_3} + \cdots\right]^2,$$

where the integers n_+ and n_- count how many times the masses M_+ and M_- appear, respectively. The number of thresholds grows with the number of loops and so does the

JHEP06(2017)066

number of disjoint regions $\tilde{\mathcal{A}}_i$ and $\mathcal{A}_i$. The thresholds that are relevant to the calculations of the physical amplitudes are those that are located on the real axis, which are

$$p^2 = (\sqrt{2}nM + m_{i_1} + m_{i_2} + m_{i_3} + \cdots)^2,$$

where $n = n_+ = n_-$.

We expect that the arguments of sections 3 and 4 for the calculation around the LW pinching work in any diagram. In a generic Lorentz frame, the regions $\tilde{\mathcal{A}}_i$ are enlarged. Lorentz invariance is violated and the integration domain on the loop space momenta must be deformed to recover it. Consider the behavior of a loop integral around some LW pinching. During the domain deformation, the deformed surface $\tilde{\mathcal{A}}_P^{\rm def}$ eventually becomes a thin strip almost squeezed onto the real axis above the LW threshold P. If τ denotes a coordinate for the long edge of the strip and η a coordinate for the perpendicular edge, while $\tilde{p}_s$ measures the length of the short edge, the denominator of (4.10) appears to capture the most general behavior we can meet (p^0 being replaced by $p^0 e^{i\varphi}$, φ small). Then, formula (3.11) is also expected to hold, as well as Lorentz invariance and analyticity above the LW thresholds.

The analytic regions $\mathcal{A}_i$ are determined as follows. Working in a generic Lorentz frame, we find the regions $\tilde{\mathcal{A}}_i$ by integrating on the natural, real domains of the loop space momenta [see figure 10]. Decomposing the propagators as in formula (3.9), we isolate the contributions $\mathcal{J}_{\rm LW}(p)$ interested by the LW pinching. For each of them, we compute $\mathcal{J}_{\rm LW}(p)$ in the main region $\tilde{\mathcal{A}}_0$, which is the one that contains the imaginary axis. Then we analytically continue the result "from below", which means from smaller to larger values of the squared external momentum p^2, till we reach a LW threshold P. We proceed with the continuation above P, but here we find two different functions, $\mathcal{J}^{0+}_{\rm LW}(p)$ and $\mathcal{J}^{0-}_{\rm LW}(p)$, depending on whether we continue from the half plane with $\mathrm{Im}[p^0] > 0$ or the one with $\mathrm{Im}[p^0] < 0$. By formula (3.11), the final outcome $\mathcal{J}^{>}_{\rm LW}(p)$ to be assigned to $\mathcal{J}_{\rm LW}(p)$ above P, is the average of $\mathcal{J}^{0+}_{\rm LW}(p)$ and $\mathcal{J}^{0-}_{\rm LW}(p)$. It is Lorentz invariant and can be analytically extended from the real axis to a region $\mathcal{A}_P$ whose boundary intersects the real axis only in P (see figure 12). Following these directions, we obtain $\mathcal{J}^{>}_{\rm LW}(p)$ without having to go through the domain deformation process described in section 3. The procedure must be applied to every LW threshold P and can be generalized to regions that are placed above more LW thresholds at the same time. The final main region $\mathcal{A}_0$ is the complement of $\cup_P \mathcal{A}_P$.

7 Conclusions

The Lee-Wick models are higher-derivative theories that are claimed to reconcile renormalizability and unitarity in a very nontrivial way. However, several aspects of their formulation remained unclear. In this paper, we have provided a new formulation of the models that overcomes the major difficulties, by defining them as nonanalytically Wick rotated Euclidean theories. Working in a generic Lorentz frame, the models are intrinsically equipped with the right recipe to treat the pinchings of the Lee-Wick poles, with no need of external ad hoc prescriptions. The complex energy plane is divided into disconnected

JHEP06(2017)066

analytic regions, which are related to one another by a well defined, albeit nonanalytic procedure.

The nonanalytic behaviors of the amplitudes may have interesting phenomenological consequences, which may facilitate the measurements of some key physical constants of the theories, such as the scales associated with the higher-derivative terms.

Acknowledgments

We are grateful to U.G. Aglietti and L. Bracci for useful discussions.

References

[1] T.D. Lee and G.C. Wick, *Negative metric and the unitarity of the S matrix*, *Nucl. Phys.* **B 9** (1969) 209 [INSPIRE].

[2] T.D. Lee and G.C. Wick, *Finite theory of quantum electrodynamics*, *Phys. Rev.* **D 2** (1970) 1033 [INSPIRE].

[3] R.E. Cutkosky, P.V. Landshoff, D.I. Olive and J.C. Polkinghorne, *A non-analytic S matrix*, *Nucl. Phys.* **B 12** (1969) 281 [INSPIRE].

[4] R.E. Cutkosky, *Singularities and discontinuities of Feynman amplitudes*, *J. Math. Phys.* **1** (1960) 429 [INSPIRE].

[5] M.J.G. Veltman, *Unitarity and causality in a renormalizable field theory with unstable particles*, *Physica* **29** (1963) 186 [INSPIRE].

[6] G. 't Hooft, *Renormalization of massless Yang-Mills fields*, *Nucl. Phys.* **B 33** (1971) 173 [INSPIRE].

[7] G. 't Hooft, *Renormalizable Lagrangians for massive Yang-Mills fields*, *Nucl. Phys.* **B 35** (1971) 167 [INSPIRE].

[8] K.S. Stelle, *Renormalization of higher derivative quantum gravity*, *Phys. Rev.* **D 16** (1977) 953 [INSPIRE].

[9] E.S. Fradkin and A.A. Tseytlin, *Renormalizable asymptotically free quantum theory of gravity*, *Nucl. Phys.* **B 201** (1982) 469 [INSPIRE].

[10] U.G. Aglietti and D. Anselmi, *Inconsistency of Minkowski higher-derivative theories*, *Eur. Phys. J.* **C 77** (2017) 84 [arXiv:1612.06510] [INSPIRE].

[11] N. Nakanishi, *Lorentz noninvariance of the complex-ghost relativistic field theory*, *Phys. Rev.* **D 3** (1971) 811 [INSPIRE].

[12] B. Grinstein, D. O'Connell and M.B. Wise, *Causality as an emergent macroscopic phenomenon: the Lee-Wick $O(N)$ model*, *Phys. Rev.* **D 79** (2009) 105019 [arXiv:0805.2156] [INSPIRE].

[13] B. Grinstein, D. O'Connell and M.B. Wise, *The Lee-Wick Standard Model*, *Phys. Rev.* **D 77** (2008) 025012 [arXiv:0704.1845] [INSPIRE].

JHEP06(2017)066

[14] C.D. Carone and R.F. Lebed, *Minimal Lee-Wick extension of the Standard Model*, *Phys. Lett.* **B 668** (2008) 221 [arXiv:0806.4555] [INSPIRE].

[15] J.R. Espinosa and B. Grinstein, *Ultraviolet properties of the Higgs sector in the Lee-Wick Standard Model*, *Phys. Rev.* **D 83** (2011) 075019 [arXiv:1101.5538] [INSPIRE].

[16] C.D. Carone and R.F. Lebed, *A higher-derivative Lee-Wick Standard Model*, *JHEP* **01** (2009) 043 [arXiv:0811.4150] [INSPIRE].

[17] B. Grinstein and D. O'Connell, *One-loop renormalization of Lee-Wick gauge theory*, *Phys. Rev.* **D 78** (2008) 105005 [arXiv:0801.4034] [INSPIRE].

[18] C.D. Carone, *Higher-derivative Lee-Wick unification*, *Phys. Lett.* **B 677** (2009) 306 [arXiv:0904.2359] [INSPIRE].

[19] E. Tomboulis, $1/N$ *expansion and renormalization in quantum gravity*, *Phys. Lett.* **B 70** (1977) 361 [INSPIRE].

[20] E. Tomboulis, *Renormalizability and asymptotic freedom in quantum gravity*, *Phys. Lett.* **B 97** (1980) 77 [INSPIRE].

[21] L. Modesto and I.L. Shapiro, *Superrenormalizable quantum gravity with complex ghosts*, *Phys. Lett.* **B 755** (2016) 279 [arXiv:1512.07600] [INSPIRE].

[22] L. Modesto, *Super-renormalizable or finite Lee-Wick quantum gravity*, *Nucl. Phys.* **B 909** (2016) 584 [arXiv:1602.02421] [INSPIRE].

[23] D. Anselmi and M. Piva, *Perturbative unitarity of Lee-Wick quantum field theory*, arXiv:1703.05563 [INSPIRE].

JHEP06(2017)066